CONEM 2022
CONGRESSO NACIONAL DE ENGENHARIA MECÂNICA
TERESINA - PI

ABCM
XI CONGRESSO NACIONAL DE ENGENHARIA MECÂNICA
DE 07 A 11 DE AGOSTO DE 2022, TERESINA-PI, BRASIL

CONEM2022-0029
MICROSTRUCTURAL AND MECHANICAL CHARACTERIZATION OF 3104-H34 ALUMINUM ALLOY

Ricardo Zanatta Kapp, ricardo.zanatta.kapp@hotmail.com[1]
Tiago dos Santos, tiago.santos@ufsm.br[1]
Kawe Allan De Lima Goulart, kawe.lima@bruning.com.br[2]
Diego Tolotti de Almeida, diegot@bruning.com.br[2]
Cristiano José Scheuer, cristiano.scheuer@ufsm.br[1]
[1] Technology and Mechanics of Materials Group - *Department of Mechanical Engineering*, UFSM, Santa Maria, RS, Brazil.
[2] Bruning Tecnometal Ltd., 98280-000, Panambi, RS, Brazil.

Abstract: *The processing of aluminum alloys from primary stages to the final product is inherently associated with a large number of metallurgical phenomena. These phenomena promote microstructural changes, which directly affect the mechanical properties, characteristics and performance of the final component. In an effort to design related material processing routes for such alloys, the correlation between material processing, microstructural features and overall mechanical properties is required. Aiming at contributing on this subject, this work investigates the correlation between microstructural characteristics and related mechanical properties of laminated sheets of 3104-H34 aluminum alloy. Microstructural characterization is carried out using metallographic analysis and XRD technique. Mechanical properties are assessed by means of micro indentation and simple tensile tests. Microstructural characterization demonstrates that A112Fe3Si and Al6Fe intermetallic precipitates phases are present in the alloy metallic matrix. The Al6Fe-type intermetallic precipitates volumetric fraction in the cross section is higher than in the longitudinal section, which slightly increases the material hardness. The yield tensile strength, ultimate tensile strength and fracture tensile present it maximum values for specimen oriented at 45 ° in relation to the rolling direction, decreasing as the orientation decreases towards 0° and increases to 90°. Young's modulus values showed this same trend. The studied material presented a high normal anisotropy and a low planar anisotropy coefficients values, confirming its suitability for application as a raw material in deep drawing operations. Finally, the values of strength coefficient and strain hardening exponent obtained indicate the studied material high formability, and its lower propensity to suffer fracture during forming.*

Keywords: *AA 3104-H34. Microstructural characterization. Mechanical properties. Plasticity. Strain hardening*

1. INTRODUCTION

In 1997, the Kyoto protocol established global deadlines and targets for reducing greenhouse gas emissions levels – GHG, especially with regard to carbon dioxide (CO_2) and methane (CH_4) emissions. With a bold and challenging proposal, it was established that up the 2012 year, the reduction in the GHG world average emissions should reach values about of 5.2% in relation to the levels registered in 1990, even with the expansion of the economy, population increase and the consequent increase in the world vehicle fleet. In this sense, considering that CO2 - the main gas involved in the greenhouse effect problem - is a gas produced from the fossil fuels burning, it is necessary to reduce the energy demand for this matrix, so that the reduction of GHG occur consistently (Magnusson and Magnusson, 2000).

In the mobility sector (automobiles, road, agricultural, rail and other vehicles), the main way to promote it is to seek to increase the vehicles energy efficiency, aiming to reduce fuel consumption, mainly by reducing their mass. To achieve this goal, one of the commonly adopted procedures is the use of thinner sheet metal in the production of its components. However, such changes must be made taking into account the cost, safety and performance criteria's (Lajarin, 2012). Another alternative to achieve the required mass reduction corresponds to the use of aluminum (Al) and its alloys to replace steel in vehicle components (Ramalho et al., 2019). In this sense, excellent results can be achieved through the use of thin Al alloy sheets in the production of automotive parts, which has generated its growing use in the mobility sector over the past few years (Filleti, 2010).

In this context, 3XXX series aluminum alloys (AA) have been widely used in such applications, due its high mechanical and corrosion resistance, and good formability and weldability. Among the AA of these series, class AA 3104 is widely used in motor vehicle components that are in contact with chemical products, as fuel tanks; and exposed to high temperatures, as heat exchanger components (The Aluminum Association, 1998).

As a result of the need to reduce the mass of automotive vehicles components, the thickness of the sheets used in their manufacture is becoming increasingly smaller. Thus, a better manufacturing operations planning is required, in order to avoid raw material wasting during the production processes execution; and optimize the manufactured component properties. This need has led to the development of many studies aimed at improving manufacturing operations, including the aluminum sheets forming. The forming of aluminum alloys is inherently associated with a large number of metallurgical phenomena. These phenomena promote microstructural changes, which directly affect the mechanical properties, characteristics and performance of the final component. In an effort to design related material processing routes for such alloys, the correlation between material processing, microstructural features and overall mechanical properties is required. Aiming at contributing on this subject, this work investigates the correlation between microstructural characteristics and related mechanical properties of AA 3104-H34 rolling sheets.

2. MATERIALS AND METHODS

Table 1 shows the chemical composition of the Al alloy used in this research, provided by the material supplier. The Mn and Mg contents are consistent with those indicated by the Aluminum Association for the AA 3104 alloy (Mn between 0.8 and 1.4%; Mg between 0.8 and 1.3%, Cu between 0.05 at 0.25% and maximum contents of 0.8% Fe and 0.6% Si). This material was supplied in cold-rolled plate format with a thickness of 2.5 mm. This AA has H34 work hardening, that is, after hardening the material was stabilized to an intermediate strength value between annealed (O) and totally hard (H19).

Table 1. Chemical composition of AA 3104 **alloy.**

Chemical element	Mn	Mg	Cu	Si	Fe	Al
Aluminum Association	0.93	1.14	0.24	0.1	0.13	Balance

Specimens were laser machining from the commercial plate according to the geometry and dimensions indicated in Figure 1a, aiming to carry out the tensile tests. The informed geometry and dimensions were adopted in order to meet the ABNT NBR 6673, ASTM E 646 and DIN EN 10 002-1 standards. This was possible, since none of the three standards establish exact dimensions for the specimens, but minimum and maximum values, within which the specimens meet the test requirements. Specimens were machined at angles of 0, 30, 45, 60 and 90° in relation to the rolling direction (Figure 1b). Before carrying out the tensile tests, the specimens were submitted to a finishing operation by manual sanding.

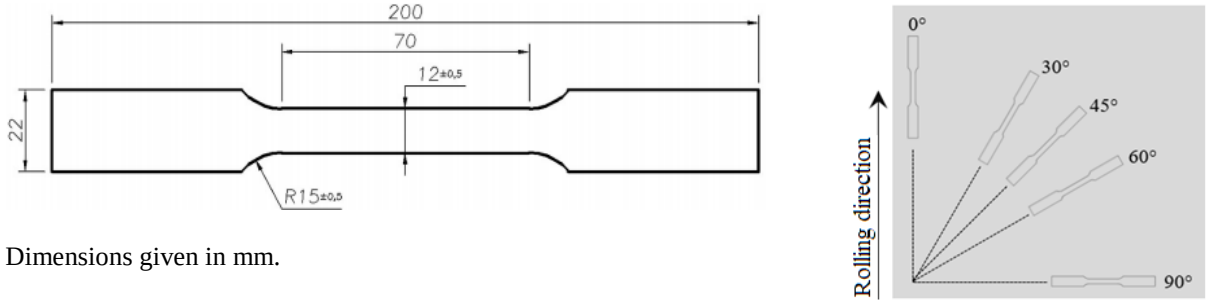

(a) (b)

Figure 1. (a) Specimens shape and dimensions adopted aiming to meet the ABNT NBR 6673, ASTM E 646 and DIN EN 10 002-1 standards for the tensile test execution. (b) Specimens orientation regarding the rolling direction.

The uniaxial tensile tests were carried out in a universal testing machine EMIC® DL100, being executed adopting a standard deformation speed of 0.5 mm/min, in accordance with previously mentioned standards. The programming of the testing machine and obtaining the load and deformation values were performed using the Tesc Emic software installed on a microcomputer interfaced to the universal testing machine. The specimens were uniaxial tensioned until rupture to obtain the engineering tension-deformation curve. With the data of the curve, using the procedures suggested by Garcia *et al.* (2012), were determined the yield (σ_e) and ultimate (σ_u) strength, the Young's modulus (E) and the percentage elongation ($\%Al$). The procedure for determining the strength (n) and the strain hardening (K) coefficients was performed following the ASTM E-646 standard. To determine the anisotropy indexes, the procedure established by the ASTM E-517 standard was followed. The presented results of the mechanical, conformability and anisotropic properties correspond to the average value of three readings.

The specimens' microstructure and microhardness were also characterized. Using the usual metallographic preparation procedures, samples of untested specimens were prepared through sanding and polishing operations using, in this order, silicon carbide sandpaper of 1200 mesh (due to the used raw material being cold-rolled, it already had a good finish), and metallographic alumina with 1.0 µm size. After preparation, the samples were attacked using Tucker reagent (200 ml of HCl; 200 ml of HNO_3; 200 ml of HF and 200 ml of H_2O), and their microstructure analyzed using an JEOL JSM 6360 scanning electron microscope (SEM). Chemical composition maps were obtained using a BrukerNano

Compact energy dispersive X-ray (EDS) spectroscopy system. These same samples were used to perform the Vickers microhardness measurements, which were performed using a Shimadzu HMU-2 microhardness meter. The microhardness measurements were performed using a 300 gf load, with a 15 s load application time. The determination of the phases present was carried out using a Bruker D8 Advance X-ray diffractometer, with CuK radiation (λ = 1.5406 Å), in the Bragg-Brentano (for 2θ angle varying on the 20-110° range) XRD configurations, using scanning speed of 1°/min.

3. RESULTS AND DISCUSSION

In Figure 2 are presented the microstructure of the AA 3104-H34 plate (a) plane and (b) cross-section. It is possible to identify the occurrence of precipitated particles dispersed in the metallic matrix. According to Connolly et al. (1997), the fine particles correspond to $Al_{12}(Fe, Mn)_3Si$ (precipitates type α) and the coarse particles constitute $Al_6(Fe, Mn)$ (precipitates type β), intermetallics that precipitate during the hot rolling operation. Note that the fine intermetallic particles frequency of occurrence is higher than that of coarse particles, indicating that the volumetric fraction of $Al_{12}(Fe, Mn)_3Si$ is higher than that of $Al_6(Fe, Mn)$. According to Coutinho (1980), the intermetallic particles precipitated that have a Cu-based constitution are light colored, those based on Mn have a shaded appearance and those based on Fe have a brownish-black color. Based on this, it can be inferred that the particles visualized in the micrographs of Figure 2 correspond to the intermetallic $Al_{12}Fe_3Si$ and Al_6Fe. It is also possible to note that the intermetallic distribution is random. It is also possible to assess that coarse particles tend to have a more elongated geometry with rounded tips, and fine particles have a different shape (elongated or equiaxed). Comparing the cross-section and longitudinal micrographs, it is observed that in the cross-section the coarse particles of the supposed intermetallic Al_6Fe present symmetry with faceted tips, and a greater volume fraction of the $Al_{12}Fe_3Si$ precipitates is observed. It is also noticed a tendency of Al_6Fe precipitates to align in the rolling direction (longitudinal axis). The $Al_{12}(Fe, Mn)_3Si$-based precipitates have high hardness compared to $Al_6(Fe, Mn)$ (Fogazzi et al., 2007), which corroborates the statement that the particles elongated in the rolling direction are Al_6Fe and the not elongated $Al_{12}Fe_3Si$.

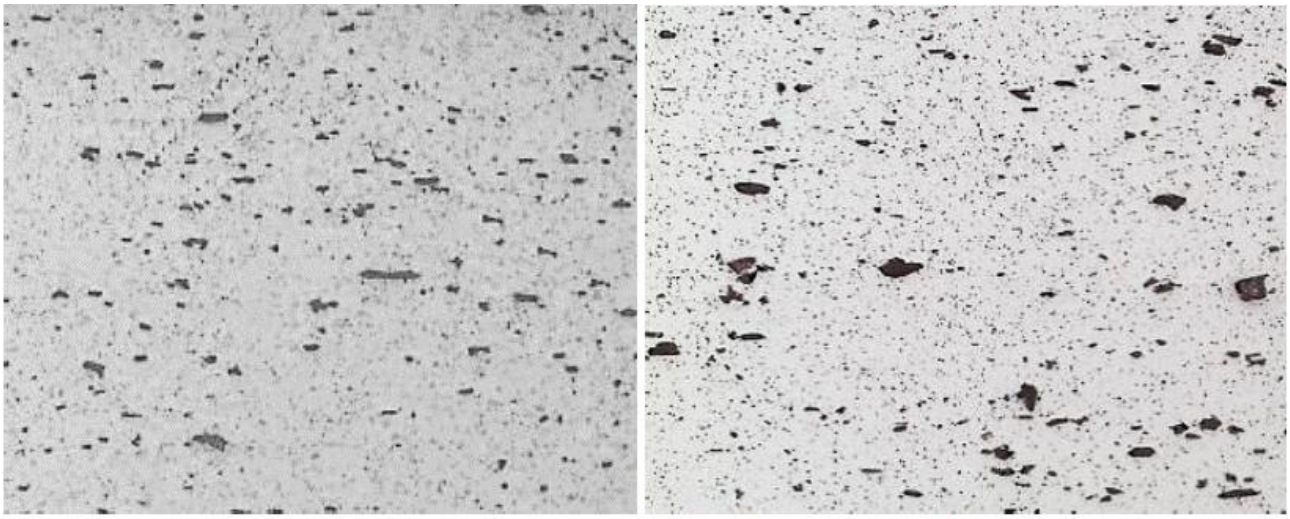

Figure 2. Microstructure of the AA 3104-H34 plate (a) plane and (b) cross-sections.

The X-ray diffraction pattern of AA 3104-H34 is shown in Figure 3. Via a comparison of ICDD (International Centre for Diffraction Data) PDF cards, it can be concluded that the present phase are α-Al, Al_6Mn and $Al_{12}Fe_3Si$, corroborating the previous discussion related to the intermetallic phases present in the material's microstructure.

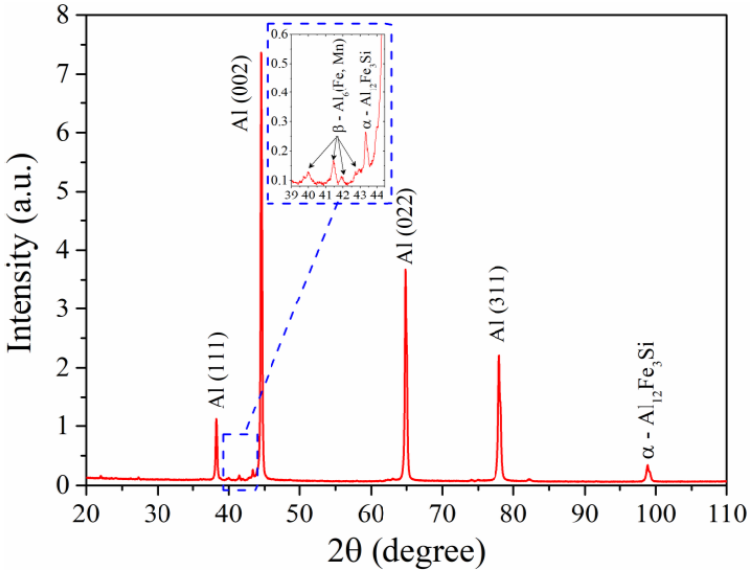

Figure 3. X-ray diffraction pattern of the AA 3104-H34 specimens.

Figure 4 shows the microhardness values measured in the longitudinal and cross sections of the specimens extracted at different angles regarding the rolling direction of the aluminum plate. The average hardness values for each orientation were very close both in the plate plane and in it cross-section, showing variations in the interval between 84 to 92 $HV_{0.3}$ in the first and 89 to 94 $HV_{0.3}$ in the second. These values are similar to those reported in the literature for the AA 3104-H19, which has an average hardness of around 88 HV (Martins, 2004). Although the mean hardness values measured in the plane and cross-section are statistically equal, it is verified that in all rolling directions the hardness in the plate cross-section is on average higher than that of the plate plane. This is possibly related to the higher volume fraction of $A11_2Fe_3Si$ intermetallic precipitates observed in the cross section micrograph (Figure 2).

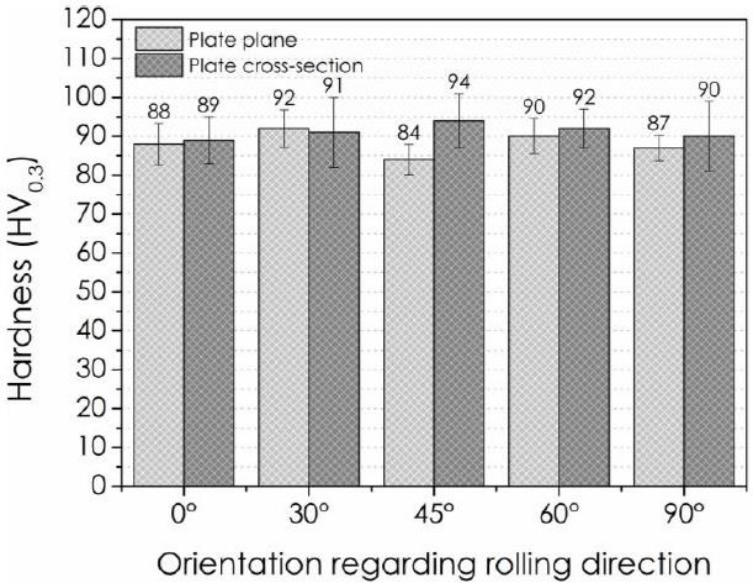

Figure 4. Hardness measured in the plane and cross-section of the samples extracted in different directions regarding the rolling direction of the AA 3104-H34 specimens.

In Figure 5 the engineering stress vs. strain curves for the specimens extracted at (a) 0°, (b) 35°, (c) 45°, (d) 60° and (e) 90° regarding the rolling direction are presented. In Figure 5 (f) is presented a comparison among all orientations. Although slight variations are observed between the curves for the same evaluated condition, in general these variations are small, within the expected interval (15%, according to Garcia et al., 2012). It is worth mentioning the occurrence of a serrated profile, observed in the segment of the engineering stress vs. strain curves in the uniform work hardening regime. This phenomenon characterizes the occurrence of heterogeneous deformations and is commonly referred to as the Portevin-LeChatelier – PLC effect (Tu et al., 2014; Cottrell, 1953). The PLC effect can be attributed to the influence of intermetallics on the discordance movement during the plastic deformation process that occurred in the uniaxial tensile test (Krishna et al., 2015; Huskins et al., 2010). During rolling, the intermetallics precipitated in the matrix are fragmented

into small particles. As shown in Figure 2, the spacing between these intermetallic particles is relatively small and therefore discordances can be trapped with them. This effect gives rise to the serrated pattern observed in engineering stress vs. strain curves of Figure 5 (Tian et al., 2019).

The analysis of Figure 5 also allows us to observe that there is no visible change in the profile of the engineering tension vs. deformation curves in the transition among elastic to plastic deformation regimes. For the case of some metals, such as low and medium carbon steels, the elasto-plastic transition is well defined and occurs abruptly, an event called the yield strength limit phenomenon (Callister and Rethwisch, 2012). For the case of aluminum and its alloys, however, the profile of the engineering tension vs. deformation follows that of the curves in Figure 5, as can be confirmed in a specific literary framework (Tian et al., 2019; Krishna et al., 2015; Huskins et al., 2010).

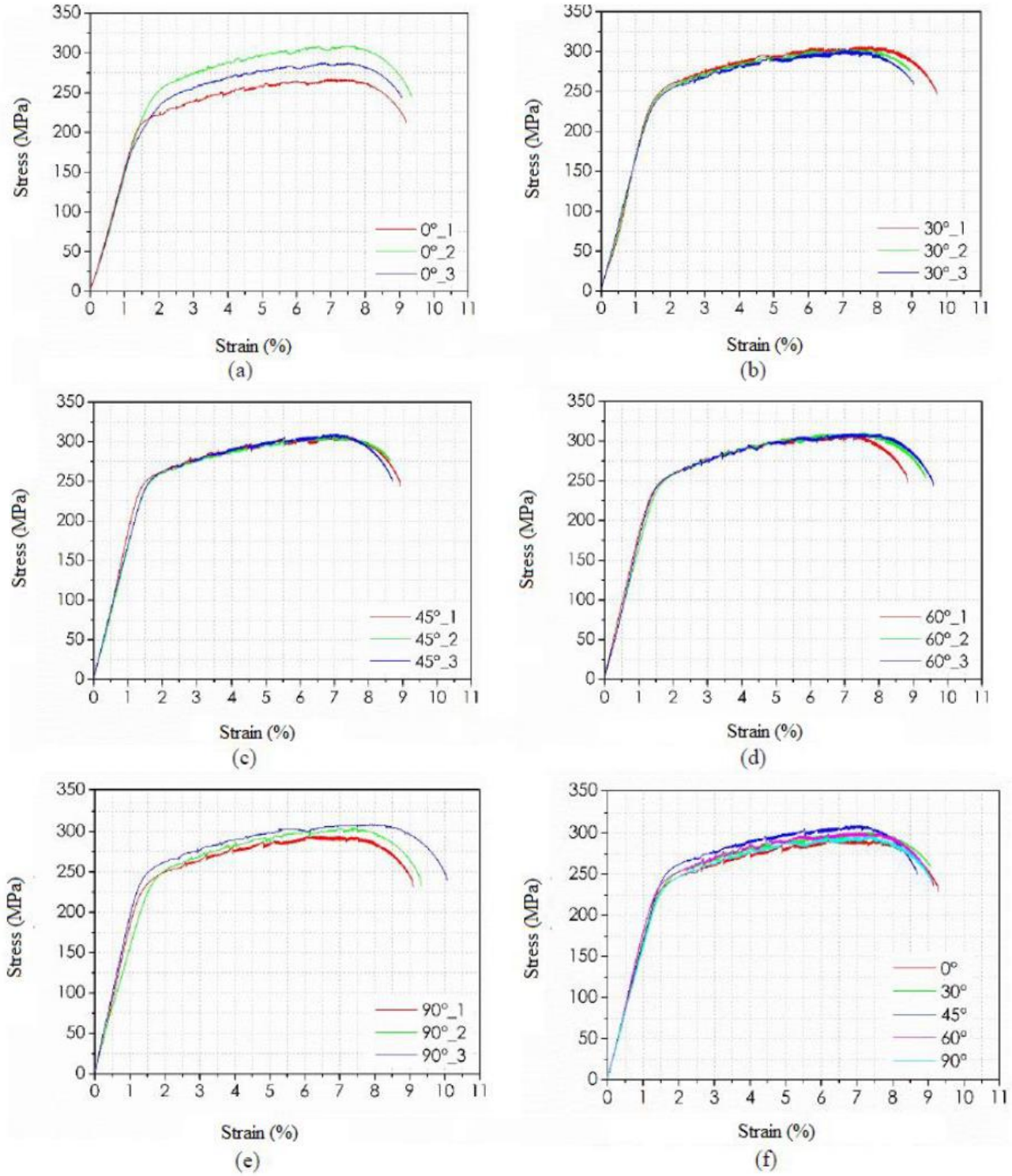

Figure 5. Engineering stress-strain curves for the specimens extracted at (a) 0°, (b) 30°, (c) 45°, (d) 60°, and (e) 90° regarding the rolling direction of the AA 3104-H34 specimens. In (f) the comparison between the curves is shown.

In the Table 2 the values of some mechanical properties determined from the stress vs. strain curve are compiled. The values of yield stress (σ_e) and tensile strength (σ_u) are slightly different from those indicated by Barbosa (2014) for class 3104 alloy submitted to H19 treatment (260 and 290 MPa, respectively). With regard to the Young's modulus (*E*), the values obtained here are equivalent to those reported by the cited reference. In the case of elongation (*%Al*), the values obtained correspond to approximately twice that value reported by the referred reference for 3104-H19. These variations in the σ_e, σ_u and *%Al* values can be credited to the differences between the treatments applied in the material studied here (H34) and that used in the material of the cited reference (H19).

Table 2. Mechanical properties regarding the rolling direction of the AA 3104-H34 alloy.

Reference	σ_e (MPa)	σ_u (MPa)	*E* (GPa)	*%Al*
0°	203,25±17	286,32±21	73,08±2,2	8,24±0,50
30°	211,01±3,7	301,57±7,0	76,33±4,8	7,78±0,36
45°	233,81±5,5	308,95±1,4	89,54±8,4	7,52±0,79
60°	230,30±2,4	302,62±2,5	85,13±4,1	7,59±0,51
90°	217,09±6,8	298,95±1,4	81,09±5,5	8,01±0,48

Table *3* presents the values of the true deformations in thickness and width (ε_{rb} and ε_{rt}, respectively) and the anisotropy indices calculated from these values. The plastic anisotropy index (r) values for the 0°, 45° and 90° orientations are similar to those reported in the literature (Chaimongkon *et al*., 2019; Barony, 2019; Mohanraj *et al*., 2021). With regard to the normal anisotropy index ($\bar{r}$), the value obtained here (0.847) is of the same order as that obtained by Barony (2019) but higher than that specified by Mohanraj *et al.* (2021) (in this order, 0.885 and 0.626). Regarding the planar anisotropy index (Δr), the value obtained in this work (0.143) is close to that indicated by Mohanraj et al. (2021) and well below the value reported by Barony (2019) (0.131 and 0.213, respectively).

Table 3. Measured plastic anisotropy indexes regarding the rolling direction of the AA 3104-H34 alloy.

Reference	ε_{rb}	ε_{rt}	r	$\bar{r}$	Δr
0°	0,064	0,015	0.2343	0,5622	0,0045
30°	0,051	0,024	0.4705		
45°	0,050	0,028	0.5600		
60°	0,045	0,028	0.6222		
90°	0,038	0,034	0.8947		

Comparing the data presented in Table 2, it is possible to observe a clear tendency to increase the values of *E*, σ_e and σ_u as the specimens cutting orientation deviates from the rolling direction until the angle of 45°, with further decrease as it grows up to the angle of 90°. As detailed by Callister and Rethwisch (2012), plastic deformation in metals is mainly due to the discordance movement through slip systems. Although the stress generated in the uniaxial test is purely tensile stress, shear stress components are formed in all directions, with the exception of the directions parallel and perpendicular to the direction of the tensile stress. The values of the shear stresses differ in each slip system present in the metal crystalline lattice, having their maximum value in the direction of 45° in relation to the direction of load application (critical shear stress), and gradually reducing towards the 0° and 90° orientations. Thus, considering that the elongation produced by the rolling guides the slip systems in the direction of plastic deformation, it is assumed that for the specimen extracted at an angle of 0° regarding to the rolling direction, its slips systems are aligned with the direction of load application in the uniaxial tensile test, being subjected to critical shear stress. On the other hand, for the direction of 90° regarding to the rolling direction, the critical shear stresses tend to cause the atomic planes separatiom than their slipping. Under this reasoning, the lowest values of the critical shear stresses would occur in the orientation of 45°, thus justifying the supposed greater resistance to plastic deformation indicated in the data in Table 2.

Table 3 presents the result of the anisotropic properties determination. The values of the anisotropy indices for each direction (r), and the mean ($\bar{r}$) and planar (Δr) anisotropy coefficients obtained here are similar to those reported by Martins et al. (2016) and Ren et al. (1994) for grade 3104-H19 aluminum alloy. According to Bresciani Filho et al. (2011), high values of $\bar{r}$ indicate that the material will resist deformation in the thickness direction, while low values of Δr indicate that the material will behave similarly in different deformation directions and, therefore, will have a lower tendency of earring-type defect formation. Based on this, the ideal materials for deep drawing process should have the lowest possible value Δr and, at the same time, the highest possible value of $\bar{r}$, thus suggesting that it will have a low tendency to form "ears" and will resist deformation in its thickness, delaying the occurrence of breakup. Considering that the material here characterized presented a low Δr value and a high $\bar{r}$ value, it can be stated that it is suitable for applications in deep drawing operations.

Table 4. Strength (*n*) and strain hardening (*K*) coefficients values regarding the rolling direction of the AA 3104-H34 alloy.

Reference	*n*	R^2	*K* (MPa)
0°	0.1127±0.009	0.9991	328.5±2.27
30°	0.119±0.008	0.9986	328.91±2.646
45°	0.1097±0.019	0.9955	327.48±0.631
60°	0.1137±0.003	0.9992	328.09±2.018
90°	0.132±0.002	0.9994	334.23±2.479

By definition, the *K* value quantifies the level of resistance that the material exerts against its deformation, that is, the higher its value, the greater the effort required to promote its permanent deformation. The *n* value, on the other hand, represents the material's ability to distribute deformation throughout its volume. Thus, materials with a low *n* value tend to localize work hardening in small volume portions, causing low levels of deformation to bring the material to conditions closer to fracture than those observed in materials with higher work hardening coefficients. In addition, low *n* values characterize large strain variations promoted by relatively small variations of the stress in the plastic zone (GARCIA et al., 2012). It is important to clarify that both coefficients are dependent on the thermal, mechanical and/or chemical treatments performed on the material; for this reason the divergence between the values obtained here in relation to those reported for the same alloy submitted to another mechanical treatment, and in relation to annealed aluminum. It is worth mentioning that the lowest *K* values obtained indicate that the AA 3104-H34 alloy studied here indicates its lower resistance to plastic deformation, evidencing its better formability in relation to the same alloy submitted to the H19 treatment. In turn, the highest value of *n* identified for the alloy submitted to the H34 treatment evidences its greater capacity to distribute the work hardening over a larger volume of material, reducing the material's tendency to fracture during the deep drawing operation.

From the results obtained above, the *n* and *K* values were substituted in the Hollomon equation, in order to describe the real plastic behavior of the studied alloy in each orientation. In this way, it is possible to know in an approximate way what the behavior of the material if the “bumpiness” were corrected and the continuation of work hardening due to the deformation could be expressed by the test. In Table 5it is possible to observe the resulting equations for the true stress as a function of the strain in each direction.

Table 5. Hollomon equations to describe the plastic behavior of class the AA 3104-H34 regarding its rolling direction.

Condição	0°	30°	45°	60°	90°
$\sigma_v : K \cdot \varepsilon^n$	$\sigma_v : 248{,}98 \cdot \varepsilon^{0.0993}$	$\sigma_v : 249{,}13 \cdot \varepsilon^{0.1025}$	$\sigma_v : 254{,}79 \cdot \varepsilon^{0.1053}$	$\sigma_v : 253{,}75 \cdot \varepsilon^{0.1014}$	$\sigma_v : 246{,}70 \cdot \varepsilon^{0.1011}$

As expected, it is noted in Figure 6 the continuation of the stress increase with the strain increase, for all orientations, due to work hardening. Although the curves profile is similar for all the rolling orientations, there is a small difference between the maximum stress found for the different orientations, since the test piece oriented at 45° regarding to the rolling direction had a K slightly higher than the others, a fact reflected in its true stress vs strain curve as shown in Figure 6.

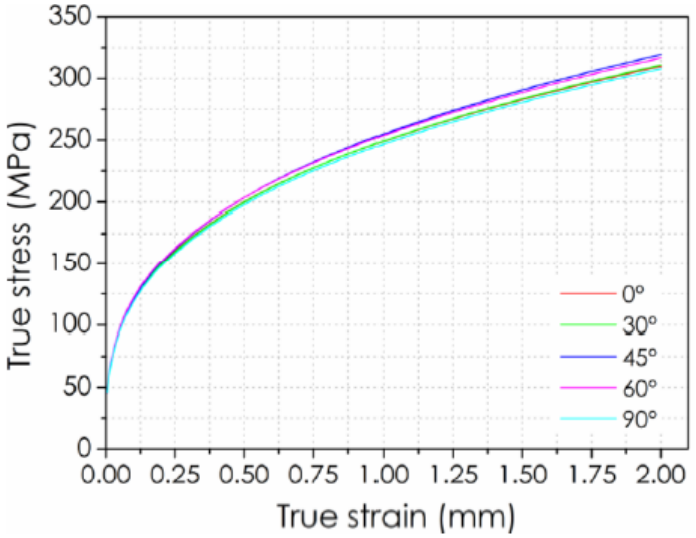

Figure 6. True stress–strain curves of AA 3104-H34 alloy.

4. CONCLUSIONS

From the analysis and discussion of the presented results, it is possible to list the following conclusions:

- The microstructure of AA3104-H34 is constituted by fine particles of $A1_{12}Fe_3Si$ precipitates and coarse particles of Al_6Fe precipitates, randomly distributed in the metallic matrix;
- $A1_{12}Fe_3Si$-type intermetallic precipitates have a more elongated geometry with rounded ends in the longitudinal section and faceted ends in the cross section; while Al_6Fe-type intermetallic precipitates exhibit equiaxed symmetry both in cross-section and longitudinal;
- The Al_6Fe-type intermetallic precipitates volumetric fraction in the cross section is higher than in the longitudinal section, which slightly increases its microhardness;
- The yield stress and tensile strength have their maximum value for the specimen oriented at 45° regarding the rolling direction, decreasing as the orientation decreases towards 0° and increases to 90°. Young's modulus values showed this same trend;
- The material presented a high mean anisotropy coefficient ($\bar{r}$) and a low planar anisotropy value (Δr), confirming its suitability for application as a raw material in deep drawing operations;
- The obtained values of strength and strain hardening coefficients indicate the high formability of the material studied, and the lower propensity to suffer fracture during its formation; and,
- The true stress vs. strain curves show a similar behavior between the different evaluated conditions, indicating a slightly greater resistance to deformation in the 45° orientation regarding to the rolling direction.

5. ACKNOWLEDGEMENTS

The authors are grateful to Bruning Tecnometal Ltd. for providing the AA 5052-H32 and specimens machining.

6. REFERENCES

Callister, W.D., Rethwisch, D.G., 2012. *Ciência e engenharia de materiais: uma introdução (in Portuguese)*. 8th ed. Editora LTC, São Paulo.

Barbosa, C., 2014. *Metais não ferrosos e suas ligas: microestrutura, propriedades e aplicações (in Portuguese)*. 1st ed. E-papers, Rio de Janeiro.

Bresciani Filho, E., Silva, I. B., Batalha, G. F., Button, S. T. *Conformação Plástica dos Metais*. 1ª. ed. São Paulo: EPUSP, 2011.

Callister, W.D., Rethwisch, D.G., 2012. *Ciência e engenharia de materiais: uma introdução (in Portuguese)*. 8th ed. Editora LTC, São Paulo.

Connolly, B.J., Lillard, R.S., Scully, J.R., Stoner G.E., 1997, "Water Staining of Al 3104-H19 Can Body Stock: A Crevice Corrosion Study Utilizing the Double Crevice Assembly Test Method". Corrosion, Vol. 53, p. 644–656.

Coutinho, T.A., 1980. *Metalografia* de *não-ferrosos:* análise e prática *(in Portuguese)*. Editora Blücher, São Paulo.

Cottrell, A., 1953. LXXXVI: A note on the Portevin-Le Chatelier effect. The London, Edinburgh, and Dublin Philosophical Magazine and Journal of Science, Vol. 44, p. 829–832.

Dieter, G.E., 1981. *Metalurgia Mecânica (in Portuguese)*. 2th ed. Ed. Guanabara Dois, Rio de Janeiro.

Filleti, A, 2010. *(web publications)* "*As novas aplicações para o Alumínio na indústria automotiva*" *(in Portuguese)*. Materiais automotivos e nanotecnologia. https://docplayer.com.br/5884674-As-novas-aplicacoes-para-o-aluminio-na-industria-automotiva.html. Accessed 01 march 2021.

Fogazzi Jr, W.S., Santos, C.A., Frick, C.R., Spim, J., 2007. "Análise Microestrutural da Liga AA 3104 H19 *(in Portuguese)*. In: *4° Congresso Brasileiro de Engenharia de Fabricação COBEF2007*, Estância de São Pedro, Brazil.

Garcia, A., Spim, J.A., Santos, C.A., 2012. *Ensaios dos Materiais (in Portuguese)*, 2th ed. Editora LTC, Rio de Janeiro.

Hortigón, B., Gallardo, J.M., Nieto-García, E.J., López, J.A., 2019. Strain hardening exponent and strain at maximum stress: Steel rebar case. Construction and Building Materials, Vol. 196, p. 175-184.

Huskins, E., Cao, B., Ramesh, K., 2010. Strengthening mechanisms in an Al–Mg alloy. Materials Science Engineering A, Vol. 527, p. 1292–1298.

Korhonen, A.S., 2013. On the Work-Hardening of AA 3104-H19 Aluminum Alloy. Journal of Materials Engineering and Performance. Vol. 22, p. 505–511.

Krishna, K., Sekhar, K.C., Tejas, R., Krishna, N.N., Sivaprasad, K., Narayanasamy, R., Venkateswarlu, K., 2015. Effect of cryorolling on the mechanical properties of AA5083 alloy and the Portevin–Le Chatelier phenomenon. Materials Design, Vol. 67, p. 107–117.

Lajarin, S.F., 2012. *Influência da variação do módulo de elasticidade na previsão computacional do retorno elástico em aços de alta resistência (in Portuguese)*. Doctoral Dissertation, Graduate Program in Mechanical Engineering, Federal University of Parana, Curitiba, Brazil.

Magnusson, S.R., and Magnusson, R.C., 2000. "The Kyoto Protocol: Implications of a Flawed but Important Environmental Policy". Canadian Public Policy/Analyse de Politiques, Vol. 26, p. 347-359.

Martins, A.L.T., 2014. *Estudo comparativo de propriedades mecânicas e textura de laminados da liga de alumínio 3104-H19 (in Portuguese)*. Master's Thesis. Graduate Program in Materials, Mackenzie Presbiterian University, São Paulo.

Ramalho, R., Lisboa, C.P., Fabricio, E., Schaeffer, L., 2019 "*Uso das ligas de aluminio de alta resistencia em substituição dos aços de alta resistência*" *(in Portuguese)*. Revista Ferramental, Vol. 1, p. 12-17.

Souza, S.A., 1982. *Ensaios de Materiais Metálicos (in Portuguese)*. 5th. Editora Blucher, São Paulo.

The Aluminum Association, INC, 1998. *(web publications)* Aluminum Alloy Selection and Applications. http://www.calm-aluminium.com.au/documents/ aluminium-alloys.pdf. Accessed 01 march 2021.

Tian, N., Yuan, F., Duan, C., Liu, K., Wang, G., Zhao, G., Zuo, L., 2019. Prediction of the Work-Hardening Exponent for 3104 Aluminum Sheets with Different Grain Sizes. Materials, Vol. 12, p. 2368.

Tu, Y.Y., Qian, H., Zhou, X.F., Jiang, J.Q., 2014. Effect of Scandium on the Interaction of Concurrent Precipitation and Recrystallization in Commercial AA3003 Aluminum Alloy. Journal of Metallurgical and Materials Transactions. A Vol. 45, p 1883–1891.

7. RESPONSIBILITY NOTICE

The authors are the only responsible for the printed material included in this paper.